Journal of Engineering Mechanics and Machinery (2026)
Clausius Scientific Press, Canada

DOI: 10.23977/jemm.2026.110203
ISSN 2371-9133 Vol. 11 Num. 2

Theoretical Analysis on Large-Stroke Dry Friction Vibration and Shock Isolation Composite Structure for Satellite Launch Environment

Guan Wang[1], Houde Dong[1], Dike Hu[2], Guyue Jiao[1,*]

[1]School of Mechanical Engineering, University of Shanghai for Science and Technology, Shanghai, China
[2]Shanghai Aerospace System Engineering Institute, Shanghai, China
**Corresponding Author*

Keywords: Dry friction, vibration isolation, impact load, nonlinear damping, mechanical model

Abstract: This paper focuses on the theoretical research of dry friction vibration isolation suitable for satellite launch dynamic environment, aiming to coordinate vibration isolation and shock buffering performance under large-stroke working conditions. Based on equivalent vibration theory, a dry friction damping model is established, and the inherent resonance-free mechanism of the isolation system is analyzed theoretically. Dry friction exhibits frequency-dependent damping characteristics, which satisfy the broadband and large-stroke dynamic demands of satellite launch equipment. The resonance-free mechanism is explored to address low-frequency resonance amplification of traditional isolators, and a nonlinear composite structure with high–low friction zones is designed to adapt to both micro-vibration and strong impact conditions. For large-stroke impact responses, direct friction calculation rather than equivalent linear damping is adopted, and Duhamel's integral is used to solve transient dynamic responses. Numerical verification shows that the peak response occurs in the residual vibration stage, and dry friction continuously dissipates vibration energy. This study provides theoretical support for the design and application of the proposed composite structure for satellite launch scenarios.

1. Introduction

With the rapid development of aerospace technology, onboard precision equipment demands higher reliability and environmental adaptability. During satellite launch and operation, equipment suffers continuous vibration, transient impact and alternating temperature loads, which easily cause structural damage and performance degradation. Developing high-efficiency vibration isolation and buffering technologies for extreme aerospace conditions carries great engineering significance to improve stability and service life. Dry friction isolation and buffering structures have become a research hotspot in aerospace nonlinear vibration control. They offer excellent energy dissipation, simple all-metal construction and wide-temperature adaptability. However, current dry friction theories lack sufficient research on resonance-free isolation mechanisms, nonlinear damping

modeling and coupled impact responses. No mature design method exists for all-metal structures that meet both vibration isolation and buffering demands. This research fills the gap with clear theoretical and engineering value.

Resonance-free isolation provides a key way to suppress resonance peaks and achieve full-band vibration reduction. Yan et al. (1998)[1] first revealed the low-frequency locking effect of dry friction damping in linear systems and proved the feasibility of resonance-free isolation. Yu et al. (2016)[2] derived the unlocking frequency and optimal damping for a bilinear hysteretic dry friction model and clarified the criteria for resonance-free performance. Yu et al. (2018)[3] used the averaging method to solve the frequency-domain response of nonlinear dry friction systems and improved the resonance-free isolation theory. These studies lay a foundation for dry friction resonance-free design, but most rely on linear or simplified nonlinear assumptions. They ignore the coupling of piecewise stiffness and dry friction, so they cannot adapt to strong impact and large deformation during satellite launch.

Dry friction damping serves as a critical mechanism for impact energy dissipation and represents typical non-smooth dynamic behavior. Early studies focused on macro-slip and micro-slip models. Den Hartog (1931)[4] proposed the classic Coulomb friction model. Iwan (1961)[5] established the bilinear hysteretic friction model that accurately describes interface slip. Li et al. (2021)[6] modified the Iwan model to improve the accuracy of bolted joint modeling. For damping characteristics, Bai (2000)[7] and Lu et al. (2007)[8] put forward equivalent linearization and Fourier series methods to calculate dry friction system responses. Yu et al. (2020)[9] obtained analytical solutions for strong nonlinear systems under large impacts using segmented Duhamel integration. Donmez et al. (2020)[10] introduced dry friction into quasi-zero-stiffness systems and greatly widened the low-frequency isolation bandwidth. Cui et al. (2023)[11] introduced dry friction into inerter isolation systems. They adopted the power flow analysis and harmonic balance method to obtain steady-state response, and confirmed that reasonable utilization of inherent dry friction can broaden the effective isolation frequency band and guide the design of frictional inerter isolators.

Researchers worldwide have conducted extensive studies on nonlinear stiffness and impact buffering. Iarriccio (2025)[12] built a coupled model for high-static-low-dynamic stiffness isolators. The model integrates piecewise stiffness, viscous damping and dry friction. He used the KBM averaging method to solve primary resonance responses and clarified how stiffness preload and dry friction affect system bifurcation. Pang et al. (1993)[13] verified that quadratic-cubic gradient stiffness improves the anti-impact performance of double-layer isolation systems. You et al. (1996)[14] proved that stiffness nonlinearity dominates shock isolation performance. Wang et al. (2015)[15] improved the multi-strand spring model by introducing nonlinear stiffness. Han et al. (2016)[16] established a dual nonlinear model for stiffness and damping. Zhang et al. (2015)[17] proposed a nonlinear gas-liquid coupling structure. All these studies confirm that nonlinear design effectively balances the conflict between vibration isolation and impact resistance.

As an all-metal dry friction damping material, metal rubber shows unique advantages in aerospace isolation. Yu et al. (2017)[18] compared several static stiffness models and proved that the micro-element spring model accurately characterizes mechanical properties. Du et al. (2026)[19] proposed a four-parameter hysteretic constitutive model that fits nonlinear elasticity and friction damping with high precision. Li et al. (2022)[20] built a fretting wear model for metal rubber wires and supports lifetime prediction. Jiang et al. (2003)[21] and Li et al. (2003)[22] systematically studied the damping and energy dissipation mechanism of metal rubber and promoted its application in aeroengines and aerospace pipelines.

Three major methods are used to evaluate impact resistance: shock response spectrum, empirical formula and dynamic analysis. Biot first proposed the shock response spectrum to guide impact test design. Time-domain analysis uses modal superposition and direct integration methods. Frequency-

domain analysis synthesizes modal solutions to calculate responses. With the development of finite element technology, numerical simulation becomes a core tool for strong nonlinear impact problems. However, current technologies have obvious limitations. Active isolation features complex structures and high costs. Traditional passive isolation hardly balances low-frequency vibration isolation and impact resistance. No collaborative design method exists for resonance-free and dry friction damping in all-metal isolators.

Drawing on existing work, the subsequent research is arranged in three main parts. Aiming at the satellite launch dynamic environment and large-stroke working conditions, this paper first establishes the dry friction damping model and explores its resonance-free mechanism by adopting the equivalent vibration theory. It then designs a nonlinear vibration isolation and buffering structure for large-stroke vibration and impact suppression. Finally, it constructs the mechanical model of the dry friction vibration isolation system under impact loading conditions. The detailed research content is presented in the following sections.

2. Dry friction damping modeling and resonance-free mechanism based on equivalent vibration theory

Dry friction occurs at the interface between two bodies when no lubricant or protective film is present, a phenomenon belonging to non-smooth dynamics. Engineering practice, however, makes perfectly sealed contact surfaces almost unattainable: oxidation layers and oil traces frequently appear and act as lubricants. Therefore, ideal dry friction studies conventionally assume no deliberately added lubricants, not perfectly uncontaminated surfaces. Initial research centered on low-dimensional structural models; later, attention shifted to dry friction damping in mechanical systems. As mechanical industry developed rapidly, complex equipment demanded ever higher dynamic performance, pushing dry friction behavior into deeper scrutiny.

Because dry friction damping mechanisms differ markedly across interfaces, both physical and mathematical models must be examined microscopically and macroscopically. Model-building rules stay largely uniform across fields: build simple yet realistic models, then assess how each parameter affects target variables. Macroscopically, friction is captured by the gross slip model; microscopically, by the micro-slip model. The gross slip model splits into two main forms: the Sgn model and the bilinear hysteretic friction model. The Sgn model treats the contact interface as uniformly conditioned, reducible to a single contact pair. The bilinear hysteretic model differs in one respect—relative sliding does not start suddenly. Below the critical friction threshold, the interface acts like a tiny spring undergoing slight elastic deformation; the surfaces stay macroscopically still yet vibrate. Once excitation exceeds critical friction, the interface unlocks and sliding begins.

The micro-slip model describes the interface through multi-point contact, involving some slip pairs and some stick pairs. Their ratio depends on tangential load magnitude. At low loads, both types coexist; as load grows, stick pairs gradually turn into slip pairs. Under certain conditions, the multi-point model may be viewed as multiple gross slip models connected in series or parallel. The parallel form expresses friction as a function of displacement, finding wider use in engineering.

Broadly speaking, the simplest model that captures main features should be chosen for a given problem. In vibration isolation and shock absorption systems, the point-to-point contact model prevails for dry friction damping—its structure is simple, parameters are clear, and it suits dynamic analysis well.

Upon comparative analysis of the characteristics exhibited by existing dry friction damping models, this project establishes a multi-parameter dry friction damping model, as illustrated in Figure 1. In this model, F_{he} and F_{ve} denote the external excitation forces acting in the horizontal and vertical directions, respectively, while F_t represents the time-varying external force.

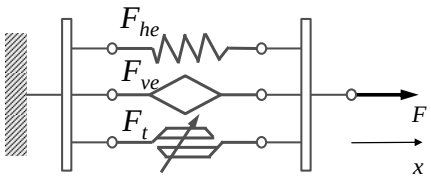

Figure 1. Multi-parameter theoretical model of dry friction

Consider a classical single-degree-of-freedom vibration system. Replacing the conventional damping term with a dry friction damping term yields the following equation of motion for the system:

$$m\ddot{x}(t) + kx(t) + f = P(t) \tag{1}$$

$$f = \mu N\, sgn(\dot{x}) \tag{2}$$

In Eq. (1), f denotes the dry friction force of the isolation system, and P(t) represents the external excitation force. In Eq. (2), μ stands for the kinetic friction coefficient, N is the normal pressure at the contact surface, and $\mathrm{sgn}(\dot{x})$ signifies the sign function.

When the system is subjected to an external displacement excitation $y = B_0 \sin(\omega t)$, the resulting steady-state displacement response is $x(t) = B\sin(\omega t - \varphi)$, where B_0 and B denote the displacement amplitudes of excitation and response, respectively.

In a dry friction isolation system, the damping contribution from springs is negligible; only the dry friction force performs negative work. Letting C_e represent the equivalent damping of the system, the negative work over one cycle can be expressed as:

$$W_c = \oint c_e \dot{x}^2(t)\, dx = \pi c_e B^2 \omega \tag{3}$$

According to the energy method, the energy dissipated by the damper in one cycle equals the mechanical energy dissipated by the dry friction vibration isolation system. The direction of dry friction force *f* is always opposite to the velocity direction of the system. The energy dissipated in a quarter cycle is denoted as *fB*, and the total energy dissipated in the full cycle is 4*fB*.

Based on the equivalent viscous damping theory, the energy dissipated by viscous damping in one cycle is supplied by the energy dissipated via dry friction damping, which gives the equality $\Delta E = 4fB$. Therefore, the equivalent damping can be derived as:

$$c_e = \frac{4fB}{\pi\omega B^2} = \frac{4f}{\pi\omega B} \tag{4}$$

Equation (4) shows that the equivalent damping coefficient C_e decreases gradually as the excitation frequency ω rises. The classic vibration transmissibility curve shows that larger damping leads to better resonance suppression in the low-frequency resonant range. Smaller damping brings better isolation performance in the high-frequency isolation range. The equivalent damping of dry friction meets this requirement well. Under the same friction force, the equivalent damping stays large at low frequencies and becomes small at high frequencies. This feature makes dry friction very suitable for vibration isolation design.

In aerospace applications, equipment operates over a wide frequency range. Traditional vibration isolation methods inevitably cause resonance within a specific frequency ratio range $\lambda < \sqrt{2}$. Classical isolation only takes effect when the frequency ratio $\lambda > \sqrt{2}$, leading to resonance amplification at low frequencies.

The dry friction isolator studied in this work shows a resonance-free feature. It solves the engineering problem of resonance failure in the low-frequency band. Yan and his group (1998)[1]

discovered the resonance-free phenomenon in engineering practice. They overturned the traditional view that resonance must occur at low frequencies. In the low-frequency band where conventional isolation fails, the transmissibility stays at unity. The load and base lock together without relative motion, and $f \geq \pi P_0 / 4$. Beyond $\lambda > \sqrt{2}$, the system directly enters the isolation region and provides stable isolation performance. No resonance peak appears across the whole frequency range, and $f < \pi P_0 / 4$. Transmissibility never rises above unity, which defines the resonance-free behavior. The corresponding transmissibility thus becomes:

$$T = \sqrt{\frac{1+(2\xi_e\lambda)^2}{(1-\lambda^2)^2+(2\xi_e\lambda)^2}} = \sqrt{(4f/\pi P_0)^2 + \frac{1-(4f/\pi P_0)^2}{(1-\lambda^2)^2}} \tag{5}$$

The vibration transmissibility expression for the dry friction isolation system is therefore given by:

$$T = \begin{cases} 1 & f \geq \pi P_0 / 4 \\ \sqrt{(4f/\pi P_0)^2 + \dfrac{1-(4f/\pi P_0)^2}{(1-\lambda^2)^2}} & f < \pi P_0 / 4 \end{cases} \tag{6}$$

In the classical vibration transmissibility curve, the frequency ratio $\lambda > \sqrt{2}$ marks the boundary between the resonance region and the isolation region. The magnitude of dry friction force governs the unlocking frequency and also affects the transmissibility within the isolation region. Therefore, optimal performance is achieved only when the system unlocks precisely at this boundary frequency: the resonance region remains locked out, while the original transmissibility in the isolation region remains unamplified. The required dry friction force at this critical point can be determined from the excitation force magnitude at the boundary frequency:

$$f = \frac{\pi}{4} B_0 m(\sqrt{2}\omega_n)^2 = \frac{\pi}{2} B_0 k \tag{7}$$

$$T = \begin{cases} 1 & \lambda \leq \sqrt{2} \\ \sqrt{\dfrac{5\lambda^2-8}{\lambda^2(1-\lambda^2)^2}} & \lambda > \sqrt{2} \end{cases} \tag{8}$$

Equation (8) works for equal displacement excitation. For equal acceleration excitation, $P_0(\omega) = mB_0\omega^2$ stays fixed regardless of frequency. So $B_0(\omega)$ varies inversely with ω^2. Under equal acceleration excitation, when the excitation frequency is sufficiently high such that the frequency ratio $\lambda \gg 1$, the transmissibility can be approximated as:

$$T = \sqrt{(4f/\pi P_0)^2 + \frac{1-(4f/\pi P_0)^2}{(1-\lambda^2)^2}} = \frac{4f}{\pi m B_0 \omega^2} \tag{9}$$

3. Nonlinear vibration isolation and buffering structure design

Dry friction isolators dissipate energy through dry friction to achieve vibration isolation and buffering. These devices feature nonlinear stiffness and damping, designed according to stiffness fitting principles and dry friction damping theory. The resonance-free isolator represents one such variant, engineered from the outset with both vibration isolation and shock resistance in mind. It eliminates resonance amplification across the entire frequency spectrum while delivering effective cushioning. To balance these dual functions within constrained design space, nonlinear stiffness and nonlinear damping must be incorporated.

In a dry friction isolator, a main spring sits inside the center post, which bolts to the load at the top.

The post bottom has a larger diameter and presses against dry friction pads to provide damping. A stiffer bottom spring boosts impact stiffness; it only engages under compression to supplement stiffness, and contacts the center post to limit travel at large displacements.

Its friction pad narrows at both ends and bulges outward in the middle, forming a larger inner diameter, as shown in Figure 2. The bottom part A of the pad is fixed, while the top part F is constrained in all degrees of freedom except the axial direction. The central column is in contact with the dry friction plate. A certain pre-compression is applied to both ends of the dry friction plate during assembly, so that its CD segment can generate friction force on the central column in the initial state. Under equilibrium and vibration conditions, the contact surface of the central column mostly moves along the CD segment. In impact conditions, however, the central column may shift to the BC and DE segments. For this reason, the BC and DE segments are designed as inclined surfaces. When the central column moves to these segments, a larger contact pressure is generated rapidly to restrain its further movement. Multiple friction pads are arranged circumferentially inside the isolator, leaving ample space for the main and bottom springs and future design changes.

According to deflection theory, the pads deform significantly when the post reaches the ends, producing high resistance; in the middle, deflection and resistance stay small. Hence the upper and lower travel regions are termed high-friction zones, and the central region the low-friction zone. Vibration excitation is typically long-duration and low-magnitude, keeping the post in the low-friction zone. Excessive friction there would increase damping and degrade isolation. Impact excitation, though brief, far exceeds vibration in magnitude. If the pad ends retained the same damping as the middle, the system would exhibit large displacement response under shock. The angled end faces instead enable rapid energy dissipation, sharply cutting displacement response. The compression mechanism maintains good isolation efficiency across varying operating conditions.

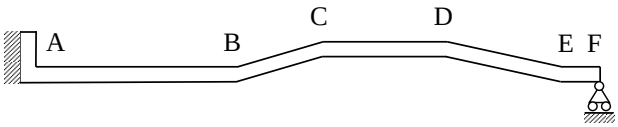

Figure 2. Schematic diagram of dry friction pad structure

When the load-connected center post reaches extreme displacement and compresses the friction pads, the pads deform substantially while the post itself remains essentially rigid.

The radial pressure on the post rises with relative displacement, and since dry friction scales with normal pressure, the friction force increases accordingly.

The deformed friction pads also exert axial pressure on the center post, and this pressure is proportional to deformation. This nonlinear axial pressure acts like a nonlinear spring, providing additional stiffness.

The center post displacement governs both axial and radial pressure. With constant kinetic friction coefficient, radial pressure determines friction force, whose direction depends solely on relative motion.

4. Mechanical model of dry friction vibration isolation system under impact loading

This section discusses the impact characteristics of the dry friction system according to the structural features of dry friction vibration isolators.

Damping force and dry friction work in the same way in vibration isolators. Both always act opposite to the direction of motion, and consume system energy by doing negative work continuously. Finite element software combined with experimental means can obtain equivalent linear viscous damping at each frequency point. However, this method only applies to cases with small vibration displacement. Impact excitation inevitably causes large system displacement, which does not satisfy

the assumption of linear viscous damping. When the center column moves to different positions, it bears different friction forces. According to its relation with motion velocity, the corresponding damping value can be theoretically equivalent. This approach still brings obvious problems. First, the equivalent damping depends on velocity, which changes with external excitation. Once the excitation condition alters, the existing equivalent damping will no longer be valid. Repeated equivalence is required to summarize the relation between damping and excitation and draw general rules. Second, the equivalent damping is nonlinear and not proportional to velocity, leading to difficult analytical solution. Even if the first problem is solved, the nonlinear feature still complicates the calculation.

In summary, introducing equivalent damping under impact load will increase the difficulty of theoretical solving. According to the Coulomb damping model, normal force remains constant, and friction magnitude only relates to position rather than moving speed. Therefore, this study adopts direct friction force calculation instead of introducing equivalent damping into the mechanical model.

4.1 Impact response of single-degree-of-freedom undamped spring-mass system

Figure 3 shows the established mechanical model. In the solution process, this paper first discusses the response of a single-degree-of-freedom undamped spring-mass system under half-sine displacement pulse excitation, as shown in Figure 3(a). The base is excited by a half-sine displacement pulse. The excitation function is expressed as follows:

$$\mathrm{u}(t) = \begin{cases} u_p \sin\left(\frac{\pi t}{\tau}\right), & 0 \le t \le \tau \\ 0 \qquad\quad , & \tau \le t \end{cases} \tag{10}$$

where u_p denotes the amplitude of displacement pulse excitation, and τ represents the impact duration, namely the pulse width. The differential equation of system motion is established as:

$$m\ddot{x} + k(x - u) = 0 \tag{11}$$

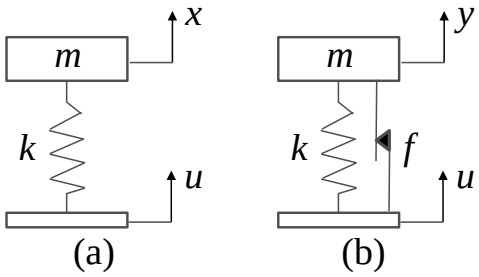

Figure 3. Mechanical model of (a) single-degree-of-freedom undamped spring-mass system, (b) dry friction buffer system

Assume the system keeps static at the initial moment t=0, with both displacement and velocity equal to zero. In linear systems, the impulse response method can solve transient vibration problems. Duhamel's integral method is extended from this approach and widely applied to transient vibration analysis. It follows the superposition principle of linear systems. The external excitation is divided into countless infinitesimal impulses, and the system responses induced by each impulse are superimposed together. Applying Duhamel's integral to Equation (11), we can obtain

$$\mathrm{x} = \frac{\mathrm{ku_p}}{\mathrm{mw_n}}\left(-\cos\left(\mathrm{w_n t}\right)\int_0^{\mathrm{t}} \sin\frac{\pi \mathrm{t}}{\tau}\sin \mathrm{w_n t_v}\,\mathrm{dt_v} + \sin \mathrm{w_n t}\int_0^{\mathrm{t}} \sin\frac{\pi \mathrm{t_v}}{\tau}\cos \mathrm{w_n t_v}\,\mathrm{dt_v}\right) \tag{12}$$

The excitation takes the form of a piecewise half-sine function. We calculate the transient response through piecewise integration and derive the following results:

$$x = \frac{u_p}{1-T^2/4\tau^2}\left(\sin\frac{\pi t}{\tau} - \frac{T}{2\tau}\sin w_n t\right) \quad (0 \le t \le \tau) \tag{13}$$

where $T = 2\pi/w_n$, w_n denotes the natural circular frequency of the system, and T represents its natural period.

When $\tau \le t$, the system enters the residual vibration stage and follows an undamped free vibration model. Its response solution is expressed as:

$$x = x_\tau \cos w_n(t-\tau) + \frac{\dot{x}_\tau}{w_n}\sin w_n(t-\tau) \ (\tau \le t) \tag{14}$$

where x_τ and $\dot{x}_\tau$ stand for the displacement and velocity of the system at the end of the impact load. Finally, we rearrange Equation (14) into the following form:

$$x = u_p \frac{(T/\tau)\cos(\pi\tau/T)}{\left(T^2/4\tau^2\right)-1}\sin w_n(t-\tau/2) \ \ (\tau \le t) \tag{15}$$

4.2 Impact response of dry friction vibration isolation system

Next, the friction force is taken into consideration. A mechanical model of the dry friction vibration isolation system is established, as shown in Figure 3(b). The differential equation of motion for the system is given as follows:

$$\mathrm{m}\ddot{\mathrm{y}} + \mathrm{k}(\mathrm{y}-\mathrm{u}) + \mathrm{f} * \mathrm{sign}(\dot{\mathrm{y}} - \dot{\mathrm{u}}) = 0 \tag{16}$$

The base is subjected to a half-sine acceleration pulse excitation in the vertical upward direction. This direction is defined as the positive direction for all subsequent calculations. The corresponding pulse function can be written as:

$$\ddot{u}(t) = \begin{cases} U \cdot \sin(\frac{\pi}{\tau}\cdot t), & 0 \le \mathrm{t} \le \tau \\ 0 & \mathrm{t} \ge \tau \end{cases} \tag{17}$$

Equation(16) therefore turns into:

$$\mathrm{m}\left(\ddot{y} - \ddot{u}\right) + \mathrm{k}(\mathrm{y}-\mathrm{u}) + \mathrm{f} * \mathrm{sign}\left(\dot{y} - \dot{u}\right) = -\mathrm{m}\ddot{u} \tag{18}$$

Let $z = y - u$, where z represents the relative displacement of the load with respect to the base. The differential equation governing the relative motion can be derived as follows:

$$m\ddot{z} + kz + f * \mathrm{sign}\left(\dot{z}\right) = -m\ddot{u} \tag{19}$$

Assume the system starts from rest with $z(0) = \dot{z}(0) = 0$. Within the impact loading stage ($0 \le t \le \tau$), relevant experimental results show that the impact duration is generally very short. This leads to a small downward displacement of the isolator central column. After the impact ends, the central column keeps moving downward due to inertia. During the entire impact action period, the relative velocity satisfies $\dot{z} < 0$. As a result, the friction force maintains a fixed direction, and the dynamic differential equation of motion can be written as:

$$m\ddot{z}_1 + kz_1 = f - mU * \sin\left(\frac{\pi}{\tau} * t\right) \tag{20}$$

The equation can be regarded as the superposition of two independent excitations acting simultaneously. The friction force f is equivalent to a rectangular pulse with constant amplitude f, while $-mU * \sin\left(\frac{\pi}{\tau} * t\right)$ is treated as a half-sine pulse force. Duhamel's integral is adopted to calculate the system response under each excitation separately.With the initial displacement and initial velocity both set to zero, the analytical solution for the response in the pulse loading stage (0< t <τ) is derived as follows:

$$z_1(t) = \frac{f}{k}(1 - \cos\omega_n t) + \frac{U}{\omega_n{}^2 - \omega^2}\left(\frac{\omega}{\omega_n}\sin\omega_n t - \sin\omega t\right) \tag{21}$$

$$\dot{z_1}(t) = \frac{f\omega_n}{k}\sin\omega_n t + \frac{U}{\omega_n{}^2 - \omega^2}(\omega\cos\omega_n t - \omega\cos\omega t) \tag{22}$$

where $\omega_n = \sqrt{\frac{k}{m}}$, $\omega = \frac{\pi}{\tau}$.

After the impact load disappears, the system enters the residual vibration stage. The friction force is assumed to remain constant, and the relative displacement keeps increasing with $\dot{z} < 0$. The corresponding differential equation of motion is expressed as:

$$m\ddot{z_2} + kz_2 = f \tag{23}$$

The initial conditions of this equation are non-zero, with definite initial displacement and velocity. These parameters correspond to the motion state at the moment the impact terminates and can be solved from Equation (21) and Equation (22). This equation only describes the continuous downward motion of the central column. When the central column reaches its lower limit position, the friction force reverses direction, and the central column starts to move upward. After the friction force changes direction, the new governing equation only differs from Equation (23) in symbol, and the solution method remains basically the same. The analytical response in the residual vibration stage is derived as:

$$z_2(t) = C_3\cos\omega_n(t-\tau) + C_4\sin\omega_n(t-\tau) + \frac{f}{k} \tag{24}$$

$$\dot{z_2}(t) = -C_3\omega_n\sin\omega_n(t-\tau) + C_4\omega_n\cos\omega_n(t-\tau) \tag{25}$$

$$\ddot{z_2}(t) = -C_3\omega_n^2\cos\omega_n(t-\tau) - C_4\omega_n^2\sin\omega_n(t-\tau) \tag{26}$$

$$C_3 = -\frac{f}{k}\cos\omega_n\tau + \frac{\omega U}{\omega_n\left(\omega_n{}^2 - \omega^2\right)}\sin\omega_n\tau \tag{27}$$

$$C_4 = \frac{f}{k}\sin\omega_n\tau + \frac{\omega * U}{\omega_n\left(\omega_n{}^2 - \omega^2\right)}(\cos\omega_n\tau + 1) \tag{28}$$

Since $\tau \ll \frac{T}{2}$ and T denotes the natural period of the system, the maximum response occurs during the residual vibration stage. The relative displacement and relative acceleration both reach their peak values when the central column moves to the bottom limit position, where the relative velocity drops to zero. Set $\dot{z_2}(t) = 0$, and we can obtain:

$$t_m = \frac{1}{\omega_n}\arctan\frac{C_4}{C_3} \tag{29}$$

Substitute Equation (29) into Equation (24) to solve for the limit relative displacement z_m. Similarly, substitute Equation (29) into Equation (26) to obtain the maximum relative acceleration a_{Rmax}.

Dry friction inside the system continuously dissipates energy. After the impact disappears, no additional energy is supplied from the outside. Friction always does negative work on the system, which gradually reduces the vibration amplitude. For this reason, the relative displacement and acceleration reach their peak values when the central column first arrives at the limit position, representing the maximum response in the residual vibration stage. Given the above relation, these peak values in residual vibration are also the maximum responses throughout the whole impact process.

Moreover, the base bears no external load after the impact excitation vanishes, and its acceleration equals zero. Accordingly, the maximum relative acceleration in the residual vibration stage is equivalent to the maximum absolute acceleration, $a_{max} = a_{Rmax}$.

To intuitively observe the dynamic response characteristics of the dry friction vibration isolation system, a calculation example is presented with given structural parameters. Based on the analytical solutions derived above, numerical calculations are conducted via MATLAB to obtain the system response curves, as shown in Figure 4. The physical parameters of a dry friction vibration isolation system are set as $m = 50$kg, $k = 4.6$kg/mm, $f = 100$N. The base is excited by a vertical upward half-sine acceleration pulse with an amplitude of 10g and a pulse width of 11ms.

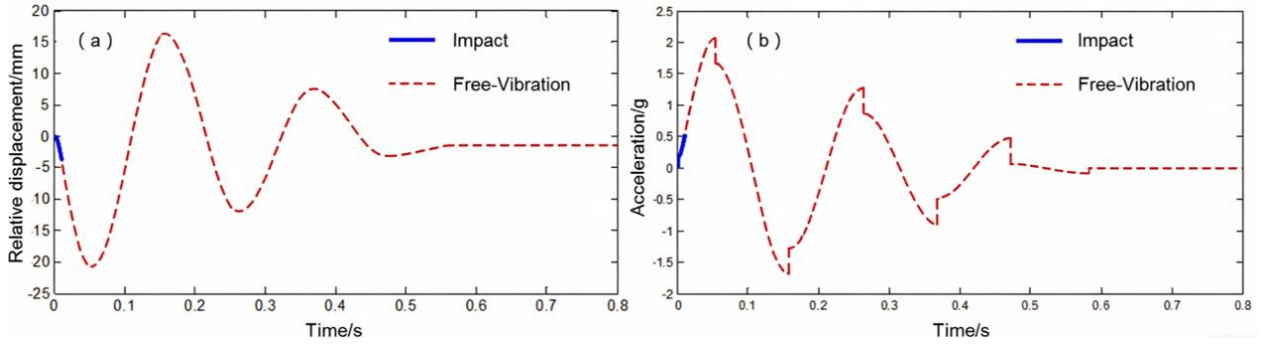

(a) Relative displacement response; (b) Acceleration response

Fig. 4 Dynamic response of dry friction isolation system in calculation example

It can be seen from Figure 4 that the displacement of the load is extremely small during the impact stage, only about 4 mm. Even with a relatively long pulse width of 11ms, the displacement generated in the impact phase will become nearly negligible if the pulse duration is further shortened. The maximum relative displacement occurs in the residual vibration stage, which agrees well with the theoretical analysis. When the pulse width is far smaller than half of the system natural period, the peak response always appears in the residual vibration process.

An abrupt change of acceleration occurs each time the load reaches its limit motion position. This phenomenon is mainly caused by the reversal of relative motion direction at the limit position, which makes the friction force change direction suddenly. In contrast, the spring elastic force remains continuous without sudden variation. The sudden reversal of friction directly changes the resultant force along the motion direction, thereby leading to an obvious jump in acceleration.

As friction continuously dissipates system energy by doing negative work, the overall acceleration gradually decays, with an equal variation amplitude at each limit position. At these extreme positions, the restoring force of the spring is lower than the friction resistance. The load slows down continuously and eventually comes to a complete stop at a certain position.

5. Conclusion

This paper investigates the dry friction vibration and shock isolation structure based on equivalent vibration theory, including damping modeling, resonance-free mechanism analysis, and impact dynamic modeling. Dry friction damping can be categorized into macroscopic gross slip and microscopic micro-slip models. The parallel micro-slip model presents better engineering applicability. The equivalent damping of dry friction decreases with increasing excitation frequency, which suppresses resonance at low frequencies and ensures effective isolation at high frequencies. The resonance-free performance depends on the matching relationship between critical frequency ratio and dry friction force. Accurate structural unlocking at the critical frequency achieves full-band resonance elimination. A nonlinear composite structure with high and low friction zones is designed to adapt to both micro-vibration and strong impact conditions by virtue of nonlinear stiffness and damping. For large-displacement impact conditions, direct Coulomb friction calculation is adopted instead of conventional equivalent damping. The Duhamel integral method is applied to solve the structural response under half-sine excitation, covering both impact and residual vibration stages. Numerical results show that the structural displacement is negligible during impact, and the maximum response occurs in the residual vibration stage. Friction reversal at limit positions causes abrupt acceleration variation, and continuous dry friction energy dissipation gradually attenuates system vibration to a static state. This study provides a theoretical basis for the design and optimization of dry friction isolation structures for satellite launch environments.

Acknowledgments

This paper was supported by Shanghai Aerospace Science and Technology Innovation Foundation (SAST2023-083).

References

[1] Yan, X.L., Ye, D.X., Zhang, Y.B., et al. Parameter Optimization of Impact Isolation for Non-Resonant Vibration Isolation Systems[J]. Electro-Mechanical Engineering, 1998(5): 37-42.
[2] Yu, H.J., Zhang, L.J. Free Resonance Analysis of Bilinear Hysteresis Dry Friction Damper[J]. Journal of Vibration and Shock, 2016, 35(12): 92-95.
[3] Yu H J, Xu Y H, Sun X T. Analysis of the Non-Resonance of Nonlinear Vibration Isolation System with Dry Friction [J]. Journal of Mechanical Science and Technology, 2018, 32 (4): 1489-1497.
[4] Den Hartog J P. Forced Vibrations with Combined Coulomb and Viscous Friction[J]. Transactions of the ASME, 1931, 53(2): 107-115. https://doi.org/10.1115/1.4022656 (published online: April 17, 2023)
[5] Iwan, W.D. The Dynamic Response of Bilinear Hysteretic Systems[D]. Pasadena: California Institute of Technology, 1961.
[6] Li, L., Wang, J.J., Shi, X.H., et al. Research on Nonlinear Modeling of Bolt Joint Surface Based on Modified Iwan Model[J]. Journal of Mechanical Engineering, 2021, 57(19): 93-101.
[7] Bai, H.B., Zhang, P.L., Huang, X.Q. Equivalent Linearization Method for Harmonic Response of Viscous Damping Hysteretic Oscillators[J]. Journal of Vibration and Shock, 2000, 19(4): 44-47.
[8] Lu, C.H., Bai, H.B., Li, D.W., et al. Response Calculation of Bilinear Hysteretic Vibration Systems with Cubic Nonlinearity and Viscous Damping[J]. Journal of Vibration and Shock, 2007, 26(1): 133-135.
[9] Yu, H.J., Wang, W.Q., Chang, W. A Solving Method for Impact Response of a Nonlinear Dry Friction System[J]. Journal of Vibration and Shock, 2020, 39(21): 111-115.
[10] Donmez, A., Cigeroglu, E., Ozgen, G.O. An Improved Quasi-Zero Stiffness Vibration Isolation System Utilizing Dry Friction Damping[J]. Nonlinear Dynamics, 2020, 101(1): 107-121.
[11] Cui, C., Shi, B.Y., Dai, W., et al. Performance Analysis of Frictional Inerter-Based Vibration Isolator[J]. Journal of Vibration Engineering & Technologies, 2023, 11(6): 2793-2817.
[12] Iarriccio, G. Primary Resonance Analysis of High-Static–Low-Dynamic Stiffness Isolators with Piecewise Stiffness, Viscous Damping, and Dry Friction[J]. Applied Sciences, 2025, 15(8): 4187.
[13] Pang, J., Yan, J.K., Shen, R.Y. Impact Response of Double-Layer Isolation System with Stiffness Nonlinearity[J].

Wuhan Shipbuilding, 1993(5): 1-5.
[14] You, G.Y., Huang, F., Wu, Q.Y. Nonlinear Anti-Impact Calculation and Analysis of Gas Turbine Base Frame[J]. Journal of Engineering for Thermal Energy and Power, 1996(S1): 50-52.
[15] Wang, S.L., Tian, B., Zhao, Y.Z., et al. Improved Shock Load Model of Stranded Wires Helical Springs Based on Perturbation Method[J]. Journal of Mechanical Engineering, 2015, 51(7): 85-90.
[16] Han, X.P., Jiang, F. Modeling for an Elastic Double-stage Vibration Isolation System with Nonlinear Shock Absorbers[J]. Noise and Vibration Control, 2016, 36(2): 31-34.
[17] Zhang, C.H., Wang, Y., Wen, Z.D., et al. Characteristics of Shock Response of a Novel Gas-Liquid Coupling Shock Damper[J]. Journal of Ship Mechanics, 2015, 19(7): 859-865.
[18] Yu, H.J., Xu, Y.H., Liu, W.H. The Comparison of Common Static Stiffness Theory Model of Metal Rubber[J]. Journal of Functional Materials, 2017, 48(11): 11141-11146.
[19] Du, Y.H., Wang, D., Hu, S.Q., et al. Hysteretic Dynamic Modeling and Vibration Characteristics Analysis of Metal-Rubber Isolators[J]. International Journal of Structural Stability and Dynamics, 2026, 26(5): 2650025.
[20] Li, H.Y., Ren, Z.Y., Huang, J.M., et al. Fretting Wear Evolution Model of the Metal Filaments Inside Metal Rubber[J]. Wear, 2022, 506-507: 204438.
[21] Jiang, H.Y., Xia, Y.H., Ao, H.R. Research on the Application of Special Metal Rubber Components Used in Aero Engine[J]. Gas Turbine Experiment and Research, 2003, 16(3): 1-5.
[22] Li, Y.M., Zheng, J., Bai, H.B. Dynamic Mechanical Model of Metal-Rubber Materials[J]. Chinese Journal of Materials Research, 2003, 17(5): 499-504.